Journal of the Korean Physical Society, Vol. 50, No. 5, May 2007, pp. 1340∼1345

Characterization of the Evanescent Field in Objective-Based Total-Internal-Reflection Fluorescence (TIRF) Microscopy

Ja Yil Lee, Shul-Kee Kim and Seok-Cheol Hong*
Department of Physics, Korea University, Seoul 136-701

(Received 28 March 2007)

Owing to its single-molecule sensitivity, objective-based total-internal-reflection fluorescence microscopy has been used to study various biological phenomena, such as conformation changes of a single biomolecule and localization and movement of single molecules inside a cell. In the technique, fluorophores associated with biomolecules are excited by an evanescent field formed near the water/coverglass interface (typically, within 100 to 200 nm). Here, we characterized the axial profile of the evanescent field. By using a prism-based scheme and applying Snell's law, we experimentally measured the incident angle of the excitation light and calculated the penetration depth of the evanescent field. The penetration depth was also acquired experimentally by measuring the fluorescence from a fluorescent bead for the excitation light at various incident angles. These independent approaches permitted highly accurate characterization of the evanescent field profile. This field profile provided the information on the distribution of the evanescent field along the axial direction, which will be useful in studying with this technique various biological phenomena as it provides a means to probe the axial dimension precisely.

PACS numbers: 42.25.B, 87.64.N, 06.30.B
Keywords: Total-internal-reflection fluorescence microscopy, Evanescent field, z distance measurement

I. INTRODUCTION

Total internal reflection fluorescence (TIRF) microscopy has been actively employed in various fields of biological research, including biochemistry, molecular biology, cell biology, and biophysics (especially single-molecule biophysics) [1–3], thanks to its high sensitivity and excellent signal-to-noise ratio. A TIRF microscope can be constructed mainly in two different ways: objective-based and prism-based systems, which are distinct in the geometry of laser excitation. The objective-based TIRF system is easier and simpler to handle because it can be readily combined with a commercial microscope without any extra components such as a prism or aligned optical components to guide the laser beam to the prism. Since both the illumination and the detection are done via one objective lens, the space above the sample chamber is not occupied by a prism or other optics, which permits using the space for other purposes, such as appending a manipulation tool to the microscope.

In TIRF, an evanescent field is established within a range of hundreds of nanometers from the water/glass interface (Figure 1(a)). This confines the observable volume to the proximity of the interface and eliminates any fluorescence from fluorophores dispersed beyond the volume. Since this confined field distribution permits excellent signal-to-noise ratio, most applications interested in single-molecule detection have utilized this advantage of the evanescent field. Another notable character of the evanescent field is that the field decays exponentially from the interface and the decay profile is characterized solely by the penetration depth. The penetration depth (δ), the distance to the interface over which the amplitude of the evanescent field decreases by a factor of e, is determined from basic electromagnetic theory:

$$\delta = \frac{\lambda}{2\pi n_{water}} \left\{ \left(\frac{\sin\theta}{\sin\theta_c} \right)^2 - 1 \right\}^{-1/2}, \qquad (1)$$

where λ is the wavelength of the excitation light in vacuum, θ_c the critical angle, and θ the incident angle.

The fact that the field decays exponentially can be very useful in analytical usage of the technique. Once we characterize the penetration depth accurately, we can measure the exact or, at least, the relative position in the vertical direction of a small fluorophore located near the interface by simply measuring its fluorescence intensity because the actual fluorescence is determined by the evanescent field profile. This benefit can be more significant when it is utilized in single-molecule spectroscopy. Single-molecule spectroscopy aims to observe only one molecule at a time to remove the ensemble average effect in bulk measurements [4–7]. In many single molecule studies, the evanescent field has been used for single-particle tracking or for measuring the distribution of

*E-mail: hongsc@korea.ac.kr; Fax: +82-2-928-3112

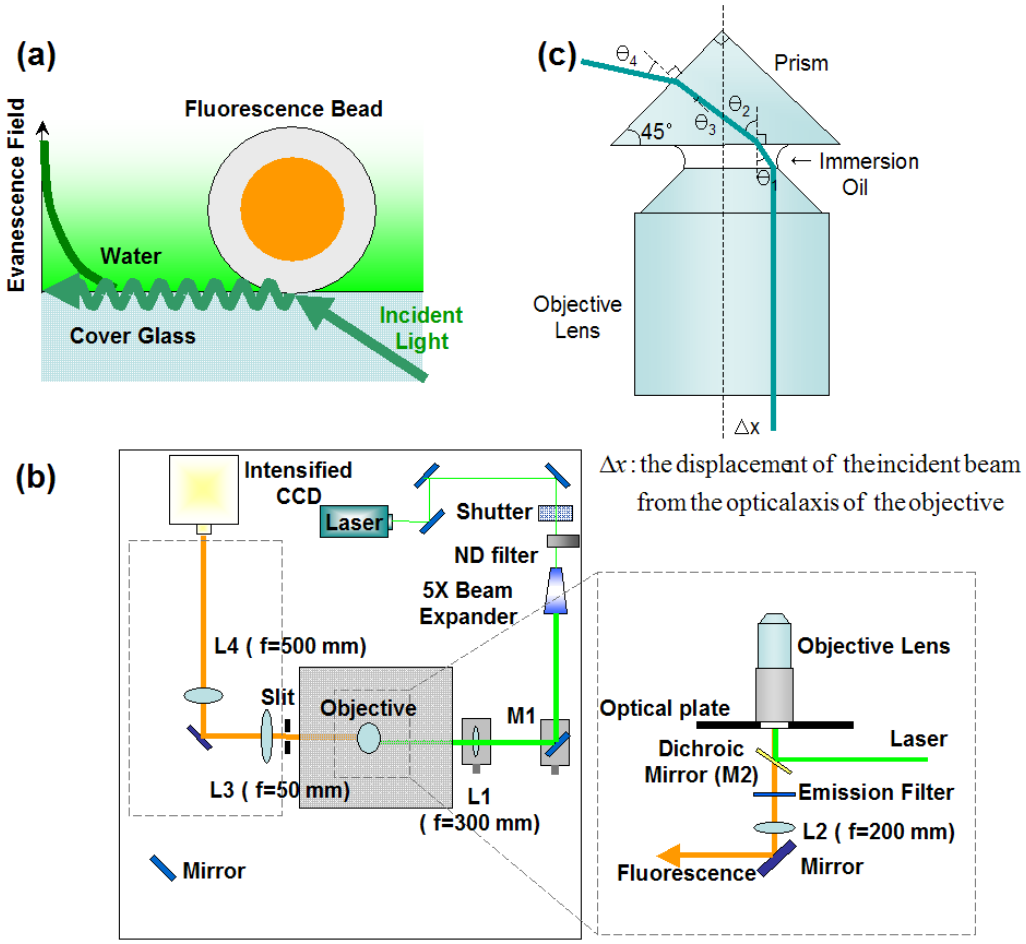

Fig. 1. (a) Evanescent field established at the water/glass interface. The evanescent field propagates along the surface and decays exponentially in the vertical direction. (b) Schematic diagram for the objective-base TIRF microscope. (c) Measurement of the incident angle from the objective lens by using a right angle prism. We measured the exit angle (θ_4) of the laser beam and calculated the incident angle (θ_1) in the oil layer by using Snell's law.

single biomolecules on a planar surface [8, 9]. The positional information about the vertical dimension could be extracted, besides the 2D image, by characterizing the evanescent field along the vertical dimension exactly.

Several attempts to characterize the evanescent field profile have been made previously. Sarkar *et al.* described the evanescent field profile by using an atomic force microscope (AFM) [10]. Either a fluorescent bead or a quantum dot was attached to the tip of the AFM cantilever, and the vertical distribution of the field was characterized from the change in the fluorescence of the particle as the height of the cantilever was changed. These measurements revealed an exponential decay of the evanescent field, which is in accord with the simple TIRF theory. Although the AFM-based characterization of the evanescent field is straightforward, its usage is often limited because of its high cost and rather complicated operation. As another approach, Mattheyses *et al.* proposed a fluorescent-bead imaging method [11]. They coated a silica microsphere with fluorescent dyes and took images of the bead exposed to the evanescent field. By analyzing the radial intensity pattern of the fluorescence image, they characterized the vertical profile of the evanescent field. This method is inexpensive and simple compared with the AFM-based one. However, it still requires labeling of the bead with fluorescent dyes and a complex technique to analyze the image.

In this paper, we propose an easier and simpler method to characterize the vertical profile of the evanescent field. Since the penetration depth is a governing parameter of the evanescent field profile and depends on the incident angle, we determined the incident angle to the cover glass by using Snell's law and a simple optical measurement in which the incident angle was evaluated by measuring the angle of the beam exiting from the prism stacked on top of an oil-immersed objective. This evanescent field profile was confirmed by another independent experiment. In this experiment, we used commercial fluorescent beads with two different diameters and imaged the beads by using an intensified charge-coupled device (CCD). The total fluorescence intensities from the beads were measured as a function of the incident angle to the cover glass. The

results with the two types of beads were fit nicely by our simple model allowing us to calculate total fluorescence signal once we knew the evanescent field profile and took a reasonable distribution of fluorescent dyes inside the beads. The consistency between the two experiments and the calculation of the penetration depth indicates that the evanescent field profile that we obtained is correct and can, therefore, be used in studying, with this technique, various biological phenomena as it provides a means to probe the vertical dimension precisely.

II. MATERIALS AND METHODS

1. Sample Preparation

Fluorescent beads with different sizes (diameter: 1 μm and 0.2 μm) were purchased from Molecular Probes. The bead suspension was diluted by 1000-fold with distilled water and dropped onto a cover glass (No. 1, Corning) placed on the objective lens.

2. Optical System for Objective-based TIRF

Fluorescence bead imaging was conducted with our home-built objective-based TIRF microscope (Figure 1(b)). Fluorescent beads were excited by using a solid-state laser (532 nm, 10 mW, Crystalaser). The laser beam was collimated and expanded by using a beam expander (BE05X, Thorlabs), reflected by using a dichroic mirror (z532RDC, Chroma: M2), and focused on the back focal plane of the TIRF objective lens (×60, NA 1.49, oil immersion, Nikon) by using a focusing lens (f = 300 mm: L1). To shift the incident laser beam to the edge of the objective lens, we simultaneously displaced the reflection mirror (M1) and the focusing lens (L1) to one side of the beam path. For precise and reproducible displacement of the two, both were mounted on a translational stage equipped with a micrometer. The fluorescence from the beads was collected by the same objective lens and focused by using an achromatic lens (f = 200 mm, Newport: L2), which played the same role as a tube lens in a microscope. To block the reflected laser light, we inserted an emission filter (HQ545LP, Chroma). After the achromatic lens, the beads were magnified 10-fold by using two combined lenses (f = 50 mm (L3) and f = 500 mm (L4), Thorlabs) and were then imaged on an EMCCD (electron-multiplying CCD, iXon BX887-BV, Andor Technology).

3. Imaging of Fluorescent Beads

Fluorescence from the beads was imaged by using an EMCCD with an exposure time of 0.1 sec. To make the collection efficiency constant, we focused the image at the critical angle by moving the objective vertically and then fixed its position. At each incident angle set by the positions of M1 and L1, five images were taken for averaging. To reduce photobleaching of the fluorescence beads, we increased the gain of the EMCCD to 4,000 and reduced the laser intensity to the optimal signal at the critical angle.

For quantitative analysis, fluorescence images converted to ASCII format were analyzed by using commercial software, IDL 6.0 (ITT Corporation). The total fluorescence intensity was evaluated by fitting the distribution of the fluorescence intensity of a bead with a 2-D Gaussian function and by calculating the volume under the function.

III. RESULTS AND DISCUSSION

1. Incident-angle Measurement by Using a Prism

Figure 1(c) shows a schematic diagram for the incident angle measurement with a prism. A right-angle prism (BK7, Thorlabs) was placed on the objective lens with immersion oil (n = 1.518) filling the gap between them. The incident angle of the laser beam to a cover glass was changed by moving the mirror (M1) and the focusing lens (L1), which in turn changed the exit angle (θ_4) of the laser beam from the prism. By measuring the exit angle and calculating the incident angle (θ_1) of the beam to the cover glass by using Snell's law, we obtained the following:

$$
\begin{aligned}
& n_{oil}\sin\theta_1 = n_{prism}\sin\theta_2, \\
& n_{prism}\sin\theta_3 = n_{air}\sin\theta_4, \\
& \theta_3 = 45^\circ - \theta_2, \\
& \theta_1 = \sin^{-1}\left\{\frac{n_{prism}}{n_{oil}}\right. \\
& \qquad \left.\times \sin\left(45^\circ - \sin^{-1}\left(\frac{n_{air}}{n_{prism}}\times\sin\theta_4\right)\right)\right\}. \qquad (2)
\end{aligned}
$$

Here, we used the following refractive indices for each layer:

n_{air} = 1.0008, n_{prism} = 1.519574 (BK7), and n_{oil} = 1.518.

The exit angle from the prism was directly measured as a function of the distance of the beam from the center of the objective (Δx), and the incident angle from the objective lens to the prism in the oil layer was calculated using Eq. (2) (See Figure 2(a)). The data were well fit by using a 5^{th}-order polynomial function: f = 901908.00 – 975234.57 Δx + 421500.70 Δx^2 – 91016.30 Δx^3 + 9819.07 Δx^4 – 423.38 Δx^5, R^2 = 0.9989. The reason for using such a high-order fit was to obtain a (polynomial) function that resembled the original data with sufficient accuracy. Using this fit, the distance Δx for incidence at the critical angle (60.842°) was calculated to be ∼4.46 mm.

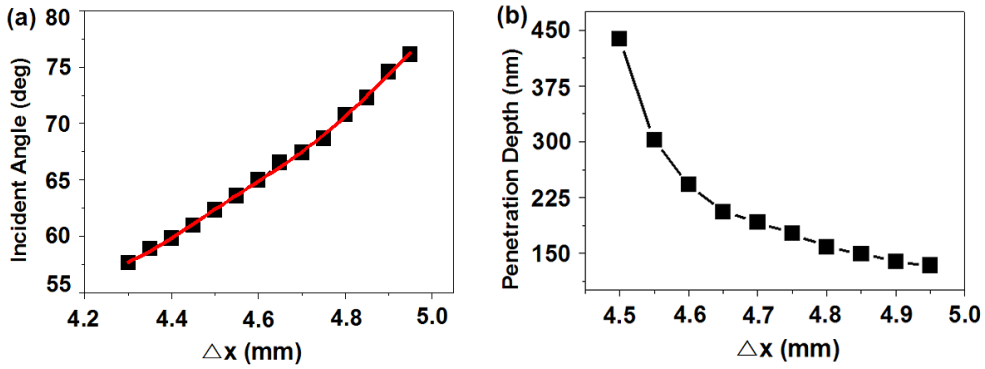

Fig. 2. (a) Incident angle of the laser beam in the oil layer as a function of the distance of the beam (Δx) from the center of the objective. The data were fit by using a 5^{th}-order polynomial function. (b) Penetration depth as a function of the distance (Δx).

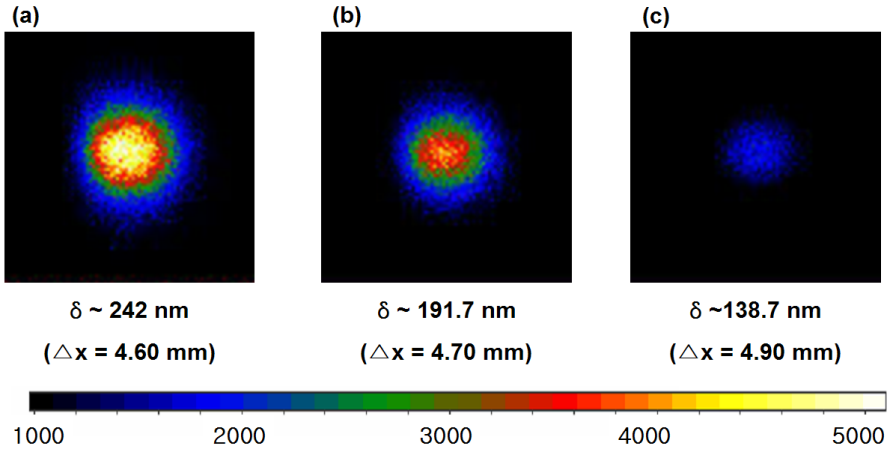

Fig. 3. Images of a fluorescent bead (1 μm) for various penetration depths (distance): (a) $\delta \sim 242$ nm ($\Delta x = 4.60$ mm), (b) $\delta \sim 191.7$ nm ($\Delta x = 4.70$ mm), and (c) $\delta \sim 138.7$ nm ($\Delta x = 4.90$ mm).

Figure 2(b) shows the penetration depth of the evanescent field as a function of the distance Δx. Using the incident angle in the oil layer (Figure 2(a)), we calculated the angle from the cover glass to the water layer and then the penetration depth from Eq. (1). These data demonstrate that we can establish the evanescent field with a specific and desired penetration depth ranging from 150 nm to 500 nm by just translating the mirror (M1) and the lens (L1). We cannot, however, tune the penetration depth finely near the critical angle because the penetration depth near that angle changes rapidly, and the micrometer that we normally use in the stage does not have sufficient resolution there.

2. Fluorescence Image and Intensity Change of Fluorescence Beads According to the Penetration Depth

Figure 3 displays fluorescence images from a single fluorescent bead with a 1-μm diameter for various penetration depths. Approximately, the fluorescence image has a 2-dimensional Gaussian profile. The fluorescence intensity and the spot size of the bead decrease as the penetration depth decreases. This is because the decrease in the penetration depth reduces the effectively illuminated volume of the bead.

Figures 4(b) and 4(c) show the total fluorescence intensities of single fluorescent beads with 0.2-μm and 1-μm diameters as functions of the penetration depth, respectively. The penetration depth was obtained as explained in Figure 2(b). The fluorescence intensity of the 1-μm bead falls more steeply than that of the 0.2-μm bead. In Figure 2(b), the penetration depth steeply decreases near the critical angle, whereas it slowly changes around 150 nm. Thus, the 1-μm bead is more sensitive to the change in effectively illuminated volume than the 0.2-μm bead, whose size is so small that most of it can still be excited even at short penetration depths.

To confirm whether the dependence of the fluorescence intensity on the penetration depth reflects a change in the evanescent field profile, we built a simple model (Figure 4(a)). We hypothesized that most fluorophores inside the bead were distributed in a shell with radius r. We do

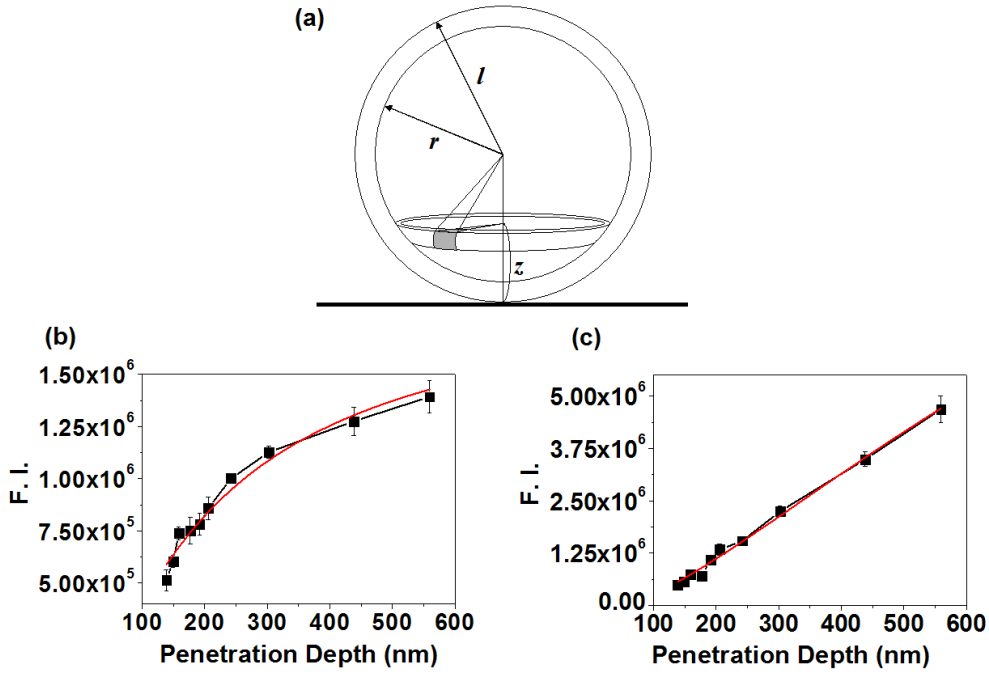

Fig. 4. (a) Schematic drawing of a shell model where most fluorophores are distributed in a shell with a specific radius (r). Fluorescence intensities (F. I.) of beads with diameters of (b) 0.2 μm and (c) 1 μm. The data were well fit by a shell model ($R^2 \sim 0.976$ and 0.995 for 0.2-μm and 1-μm beads, respectively). The shell radius of each bead was calculated to be 80.3 $\pm$ 10.9 nm for the 0.2-μm bead and 428.7 $\pm$ 6.7 nm for the 1-μm bead.

not know the exact distribution of fluorescent dyes in the bead, but it is more likely that the fluorophores spread in bulk, not in a shell. If the concentration of fluorescent dye is too high inside a bead, the compact packaging of the dyes may causes self-quenching [12], and most of the fluorescence will result from fluorescence emission of the dyes in the periphery. Therefore, the shell model should, in fact, describe the phenomena quite well. The fluorescence from a bead with a penetration depth δ can be described by using the following simple equation:

$$I = \alpha \int_{l-r}^{l+r} e^{-2z/\delta} r dz = \alpha r \delta (e^{-2\frac{l-r}{\delta}} - e^{-2\frac{l+r}{\delta}}).$$

Here, l is the bead radius, r the shell radius, and $\alpha = 2\pi I_0 \sigma \Phi \eta s$ (I_0 is the intensity at the water/glass interface, σ the extinction coefficient of the fluorescent dye, Φ the quantum yield of the dye, and η the collection efficiency of our detection system. All parameters, although not known separately, are constant and lumped into α because a laser with one specific wavelength illuminates the same type of fluorescent dyes). We assigned a shell radius (r) and a proportionality constant (α) as fitting parameters. Our model is well fit ($R^2 > 0.98$) to the data (red line in Figures 4(b) and 4(c)), and the shell radii are given as 80.3 $\pm$ 10.9 nm and 428.7 $\pm$ 6.7 nm for 0.2-μm and 1-μm beads, respectively. The acquired shell radii are not unrealistic or unreasonable because they are about 80 % of the bead radius for both cases. Fitting the total fluorescence curves in Figures 4(b) and 4(c) is highly sensitive to the value of r, which implies that, in addition, we shall be able to estimate the effective radius of the shell of the fluorescent dyes quite precisely with this method.

Since we could not obtain information about the exact distributions of the fluorescent dyes inside the beads, we had to approximate the distributions as a shell with the radius r being a fitting parameter, as mentioned. This distribution is, however, the simplest assumption we can make for the distributions of the dyes under the possibility of self-quenching. Surprisingly, this shell model explained all of our experimental results for both kinds of beads nicely and even showed a quantitative agreement on r/l of the shell between the cases with beads of different sizes. The consistency among our data makes our results and the experimental scheme we proposed more reliable.

IV. CONCLUSION

In our brief report, we have described a simple method to characterize the axial profile of the evanescent field and to determine its penetration depth. We showed that the evanescent field profile calculated from the measurement of the incident angle of the excitation light is consistent with measured values of the total fluorescence from two different kinds of fluorescent beads exposed to the same excitation light. The fact that the evanescent field

decays exponentially with a penetration depth a few hundreds nm long makes the determination of the position of the fluorescent particles possible with tens-of-nm accuracy because the fluorescence from the exponentially decaying excitation field will also show a similar exponential variation. This method will provide a useful means to probe the axial dimension precisely, which is important in applications of single-molecule techniques, such as magnetic tweezers, to various biological phenomena.

ACKNOWLEDGMENTS

This work was supported by a Korea Research Foundation (KRF) Grant funded by the Korea Government (MOEHRD, Basic Research Promotion Fund, KRF-2005-070-C00054, S.-C. H. and J. Y. L.), in part by grant No. R01-2005-000-10477-0 from the Basic Research Program of the Korea Science & Engineering Foundation (S.-C. H. and S.-K. K.), and in part by the Seoul R&BD Program (S.-C. H.).

REFERENCES

[1] A. Ishijima, H. Kojima, T. Funatsu, M. Tokunaga, H. Higuchi, H. Tanaka and T. Yanagida, Cell **92**, 161 (1998).

[2] J. Y. Lee, B. Okumus, D. S. Kim and T. Ha, Proc. Natl. Acad. Sci. **102**, 18938 (2005).

[3] M. W. Allersma, L. Wang, D. Axelrod and R. W. Holz, Mol. Biol. Cell **15**, 4658 (2004).

[4] C. Zander, J. Enderlein and R. A. Keller, *Single Molecule Detection in Solution: Methods and Application* (Wiley-VCH, Verlag, Berlin, 2002), p. 1.

[5] J. S. Park, B. Jeong, K. J. Lee, S. C. Hong, J. Y. Hyun and S. Hong, J. Korean Phys. Soc. **49**, 963 (2006).

[6] Y. Yamaguchi, Y. Maruyama, M. Ishikawa and M. Futamata, J. Korean Phys. Soc. **47**, 56 (2005).

[7] S. Weiss, Science **283**, 1676 (1999).

[8] A. Yildiz, J. N. Forkey, S. A. McKinney, T. Ha, Y. E. Goldman and P. R. Selvin, Science **300**, 2061 (2003).

[9] E. Betzig, G. H. Patterson, R. Sougrat, O. W. Lindwasser, S. Olenych, J. S. Bonifacino, M. W. Davidson, J. Lippincott-Schwartz and H. F. Hess, Science **313**, 1642 (2006).

[10] A. Sarkar, R. B. Robertson and J. M. Fernandez, Proc. Natl. Acad. Sci. **101**, 12882 (2004).

[11] A. L. Mattheyses and D. Axerlrod, J. Biomed. Optics **11**, 014006-1 (2006).

[12] S. Hamann, J. F. Kiilgaard, T. Litman, F. J. Alvarez-Leefmans, B. R. Winther and T. Zeuthen, J. Fluorescence **12**, 139 (2002).